# Spreading of Viscous Liquids at High Temperature: Silicate Glasses on Molybdenum

*Sonia Lopez-Esteban*[†], *Eduardo Saiz*[†*], *José S. Moya*[‡], *Antoni P. Tomsia*[†]

Lawrence Berkeley National Laboratory, Materials Sciences Division, Berkeley, CA 94720, USA and Instituto de Ciencia de Materiales-CSIC, Cantoblanco, 28049 Madrid, Spain

**Abstract**

The spreading of Si-Ca-Al-Ti-O glasses on molybdenum has been investigated. By controlling the oxygen activity in the furnace, spreading can take place under reactive or non-reactive conditions. As the nucleation of the reaction product under reactive conditions is slow in comparison to the spreading kinetics, in both cases the glass front moves on the metal surface with similar spreading velocities. Spreading can be described using a molecular dynamics model where the main contribution to the wetting activation energy comes from the viscous interactions in the liquid. Enhanced interfacial diffusions in low-oxygen activities (reactive cases) form triple-line ridges that can pin the wetting front and cause a stick-slip motion.

---

[†] Lawrence Berkeley National Laboratory.

[*] To whom the correspondence should be addressed. E-mail: esaiz@lbl.gov

[‡] Instituto de Ciencia de Materiales-CSIC.

**Tittle Running Head**: Spreading of silicate glasses

**Keywords:** Spreading, glass, metal, interfaces.

## Introduction

It's widely known that liquid spreading analysis is theoretically and technologically important in industry. Wetting experiments are often the only probes available to measure fundamental quantities directly linked to atomic structure and bonding at interfaces, such as the interfacial energies or the thermodynamic work of adhesion between two phases. Additionally, the progress of key technologies such as adhesives, paints, oil recovery, brazing, soldering, and many others is based on the control of liquid spreading; consequently, the study of spreading is the focus of intensive theoretical and experimental research.[1-3] The theories of spreading can be divided into two groups in which the main difference is the identification of the primary source of energy dissipation that controls the movement of the liquid front.[3-7] Continuous hydrodynamic theories focus on spreading controlled by the bulk liquid's viscous impedance[5, 8-10] while molecular-kinetic analyses describe a situation in which local dissipation at the triple line is the dominant contribution.[4, 6, 11, 12] The relative importance of each dissipation mechanism depends on a balance between the viscosity, the activation energy for viscous flow, and the strength of the solid/liquid interactions.[13] It is then imperative to test current theories against systems with a wide range of viscosities and interatomic forces. While the role of viscosity can be explored using different organic liquids at room temperature, solid/liquid interactions are much stronger during the high-temperature spreading of liquid metals and oxides. In this context, the analysis of

molten-oxide spreading is critical, because it combines both very large viscosities and strong intermolecular forces.

Most of the studies of glass spreading have focused on technologically relevant systems for which spreading is often accompanied by chemical reactions or interdiffusion at the solid/liquid interface.[14-16] The complexity of these systems makes the analysis difficult and hampers the comparison with current theories that, in most cases, describe nonreactive liquid spreading on flat substrates.

This paper focuses on a study of a simple glass/metal system that will allow a straightforward comparison with the theory. With this objective in mind, we have analyzed the spreading of $SiO_2$-CaO-$Al_2O_3$ glasses with $TiO_2$ additions on Mo. Both the silicate glass and the molybdenum have important technological applications (e.g., in glass sealing) due to their resistance to corrosion and refractory nature. Titanium additions are frequently used to enhance wetting in metal-ceramic systems.[17, 18] Most importantly, this is an excellent model system. The glasses do not have volatile components and are stable in a wide range of temperatures and oxygen partial pressures. One of the difficulties of studying high-temperature systems is the fact that the surface diffusion and solution precipitation rates of the solid are not negligible; the substrate is not ideally rigid and insoluble, therefore complicating the interpretation of the results.[19, 20] This effect can be minimized by using a substrate with a melting point well above the experimental temperature, such as molybdenum whose melting point is 2615°C. In this way, it is possible to decrease the interfacial transport rates to the point in which the substrate is effectively inert. This system has an additional advantage: by controlling the oxygen partial pressure, the interface can

be changed from non-reactive to reactive. Besides some critical oxygen activity, there is no chemical reaction or interdiffusion between the glass and the metal, but below it, they will react to form molybdenum silicides. For most technological processes, from glass sealing to soldering or brazing, spreading is accompanied by chemical reactions. The theoretical analysis of high-temperature reactive wetting is still the subject of great controversy.[17,21] Because the glass/metal reactivity can be controlled by such a simple method, this system provides a unique opportunity to ascertain how chemical reactions affect liquid spreading and to provide data fundamental to developing a comprehensive theory of reactive wetting.

## Experimental Procedure

The spreading of $SiO_2$-CaO-$Al_2O_3$-$TiO_2$ glasses (the compositions are listed in Table I) on Mo substrates was analyzed using sessile drop experiments or a drop transfer setup. The experiments were performed at 1200°C in Ar/$H_2$ flowing at ~$2 \cdot 10^{-5}$ $m^3/s$. At this temperature, the glasses are molten and behave like a highly viscous liquid. The oxygen activity was controlled by mixing Ar and Ar/1%$H_2$ in different proportions and monitored using a $ZrO_2$ sensor (Centorr, USA, model 2D). The experiments were performed at oxygen partial pressures ranging from $10^{-23}$ to $10^{-16}$ atm. These oxygen partial pressures are low enough to avoid Mo oxidation.

The Mo substrates (99.9% Aldrich, USA; 10×10×1 mm) were ground with a series of silicon-carbide paper (up to 400 grit) and polished with diamond paste up to 1 μm particle size. Subsequently, they were annealed in vacuum at 1600°C for 6 h in order to ensure that the grain boundaries intersect the surface at their equilibrium angle. The grain-boundary grooves that

formed during the heat treatment were removed by a light polishing with diamond (1 μm particle size). The glasses were prepared following a conventional procedure: the reagents $SiO_2$, $CaCO_3$, $SiO_2$, and $TiO_2$ were proportionally mixed in ethanol using a high-speed stirrer. The mixture was first dried at 80°C for 12 hours, and then fired in air at 1500°C for 4 hours in a Pt crucible. The melt was cast into a graphite mold to create glass plates, which were later cut into pieces used in sessile drop experiments and surface energy measurements. Prior to the experiments, the glass pieces and the substrates were cleaned with acetone and ethanol in an ultrasonic bath and dried with an air gun.

| | **$SiO_2$** | **CaO** | **$Al_2O_3$** | **$TiO_2$** |
|---|---|---|---|---|
| **G** | 62.00 | 23.00 | 15.00 | 0.00 |
| **GTi** | 59.63 | 22.15 | 14.42 | 3.80 |

**Table 1.** Glass compositions (in wt%). Glass GTi has an addition of 3 mol wt% $TiO_2$ compared to the composition of glass G.

In the sessile drop experiment, a small piece of glass (~2 $mm^3$ in volume) was placed on the Mo substrate inside the furnace, and the assembly was heated to 1200°C, at 25°C/min. In the drop transfer experiment, a glass piece was placed on BN substrate, and then also heated to 1200°C, at 25°C/min; subsequently, the Mo substrate was lowered from the top of the furnace towards the molten glass drop on the BN substrate until it just touched the liquid; the glass spread on the Mo substrate during the transfer from the BN substrate where it exhibited a large obtuse contact angle. In both experiments, photographs of the drops were taken, at regular intervals using a high-speed photography system able to record up to 2,000 frames per second,

through a porthole in the furnace; the drops' radius and contact angle were measured using a program developed by our group. After the required time, the furnace was shut off, and within ~15 min, it cooled down to room temperature. Averages of the contact angle from both sides of the drop were reproducible to within ± 3°.

After the tests, the samples' surfaces and cross sections were polished with 1 μm diamond and observed using optical microscopy and scanning electron microscopy with associated calibrated energy dispersive analysis (SEM-EDS). For selected samples, the glass drops were separated from the metal, and the morphology of the uncovered interface was observed by reflected light optical microscopy, SEM-EDS, Auger electron spectroscopy, and atomic force microscopy (AFM). The profiles of the boundary grooves at the solid/liquid and solid/vapor interface were measured using AFM line analysis in the constant-force mode.

The surface tension of the molten glass drops, $\gamma_v$, has been calculated from the shape of sessile drops melted on boron nitrate substrates. The measurements were performed in the same range of oxygen partial pressures used in the spreading experiments. The BN substrates and the glass pieces were ultrasonically cleaned in acetone and ethanol and air-dried before the test. A 0.20–0.25 g glass piece was placed on the BN substrate, and the assembly was heated to 1200°C at 25°C/min. The drop shape was monitored as a function of time using a CCD camera, and the corresponding surface energy was calculated using commercial software.[22]

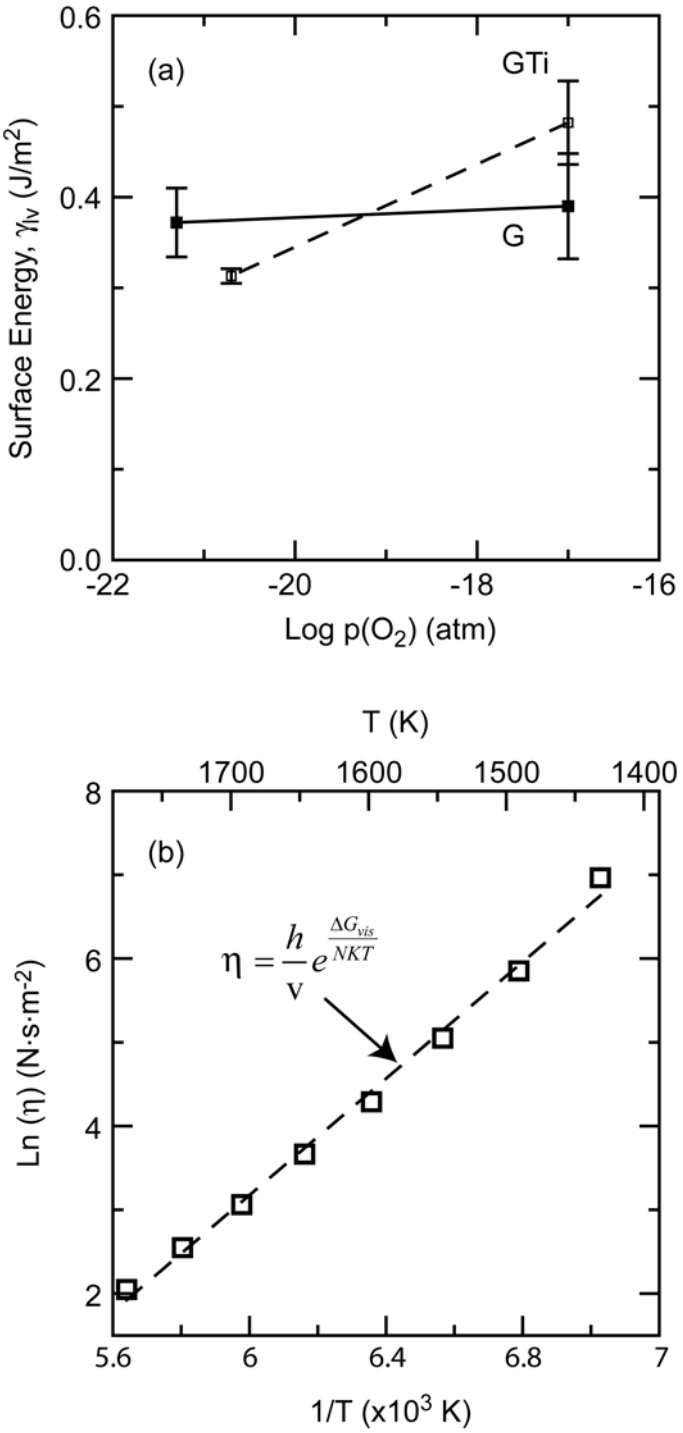


Figure 1. (a) Measured surface tensions for glasses with (GTi) and without (G) titania performed using the sessile drop method on a BN substrate. (b) Dependence of viscosity on temperature for a $SiO_2$-$Al_2O_3$-CaO glass (60-15-25 wt%), which is almost identical to the glass used in this work.[25] Fitting viscosity data to a reaction-rate equation, where v is the volume of the unit flow and $\Delta G_{vis}$ is an activation energy for bulk flow results in $v \approx 3 \cdot 10^{-26}$ m$^3$ and $\Delta G_{vis} \approx$ 290 kJ/mol

## Results

**Glasses.** The starting glasses were clear and transparent. After the wetting experiments, the glasses with $TiO_2$ always turned purple-gray, whereas glasses without $TiO_2$ remained transparent. It is well known that this color change is due to the partial reduction of titanium oxide at low oxygen partial pressures such as those used in our experiments.[23]

The measured $\gamma_{lv}$'s of the glasses at 1200°C were 0.3–0.5 J/m$^2$ (Figure 1). The surface tension increased only slightly with increasing oxygen activity. Weirauch and Ziegler reported a surface energy of 0.4 J/m$^2$ for a silicate glass of similar composition.[24] According to the reported data for glasses in the $SiO_2$-CaO-$Al_2O_3$ system, the expected viscosity of the glasses used in this work at 1200°C is ~350 N·s/m$^2$ (Figure 1).[25] The small additions of $TiO_2$ are not expected to have a significant effect on viscosity.[25]

The equilibrium oxygen partial pressure for the reaction:

$$3\ Mo + SiO_2 \rightarrow Mo_3Si + O_2(g)\uparrow \qquad (1)$$

is ~$10^{-19}$ atm at 1200°C. Consequently, there is critical oxygen activity below which glass spreading on molybdenum is accompanied by chemical reactions at the interface with silicide formation. However, for larger $p(O_2)$'s, there will be no chemical reactions or measurable interdiffusion between the glass and the metal. Reactions with the other glass components ($Al_2O_3$, CaO, or even $TiO_x$) will require even lower oxygen partial pressures.[26] Consequently, we

have used the equilibrium $p(O_2)$ for reaction (1) as an approximate value for this critical oxygen activity and divided the experiments into two types: reactive and nonreactive.

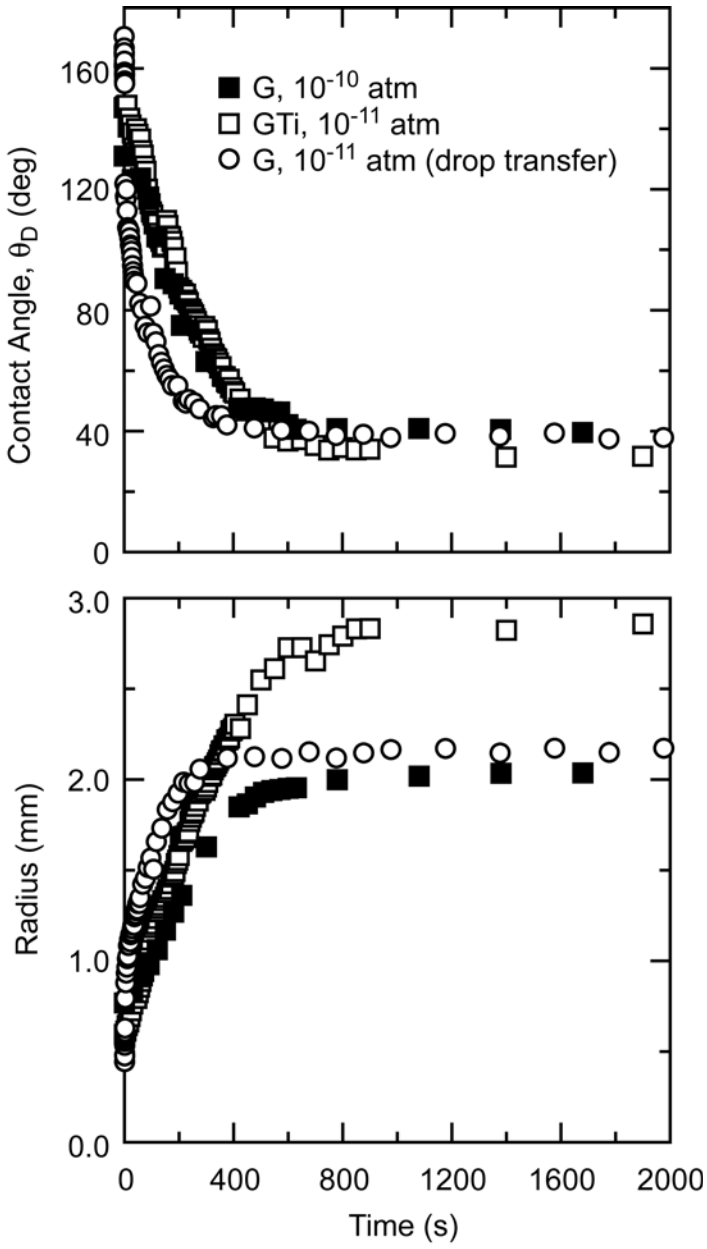


Figure 2. Evolution of the contact angle and drop radius with time for a glasses spreading on Mo at 1200°C. The oxygen partial pressure during the experiment was $10^{-16}$ atm (nonreactive conditions).

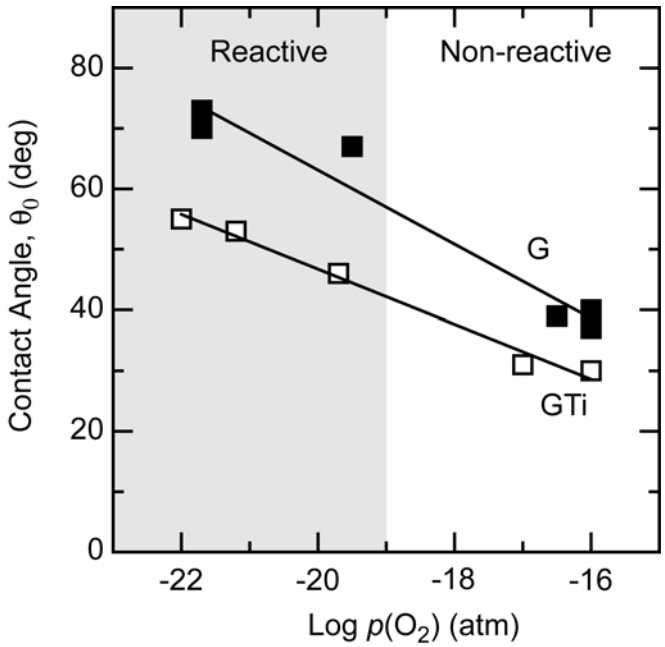


Figure 3. Final contact angles for glasses with (GTi) and without (G) titania on Mo as a function of the oxygen partial pressure. The shadowed area corresponds to the range of oxygen activities where chemical reactions between the glass and molybdenum are expected.

**Nonreactive spreading ($p(O_2)>10^{-19}$ atm).** The spreading behavior observed using the drop transfer setup and the sessile drop configuration is very similar, although in the drop transfer experiments, the initial stages of spreading (very large dynamic contact angles) can be recorded. In all cases, equilibrium contact angles were reached after 4 to 12 min (Figure 2). The equilibrium contact angles are lower for glasses with $TiO_2$ (Figure 3). The thermodynamic works of adhesion, $W_{ad} = \gamma_{lv}(1+\cos\theta_0)$, measured at a $p(O_2) = 10^{-16}$ atm, are ~0.92±0.2 J/m$^2$ for the glass with $TiO_2$, and ~0.70±0.2 J/m$^2$ for the glass without $TiO_2$.

As expected, the SEM-EDS analysis showed that there was no reaction or interdiffusion at the glass/metal interface. It was not possible to distinguish grain boundary grooves at the glass/metal interface or on the free Mo surface. After cooling, a sharp triple junction was observed. There

was no indication of the existence of a precursor foot, as it has been reported for other glass/metal systems[27], or of the formation of triple-line ridges[19, 20]. Auger analysis of the free surface of Mo and of the Mo/glass interface after removing the drop showed only a small Ca peak (Figure 4).

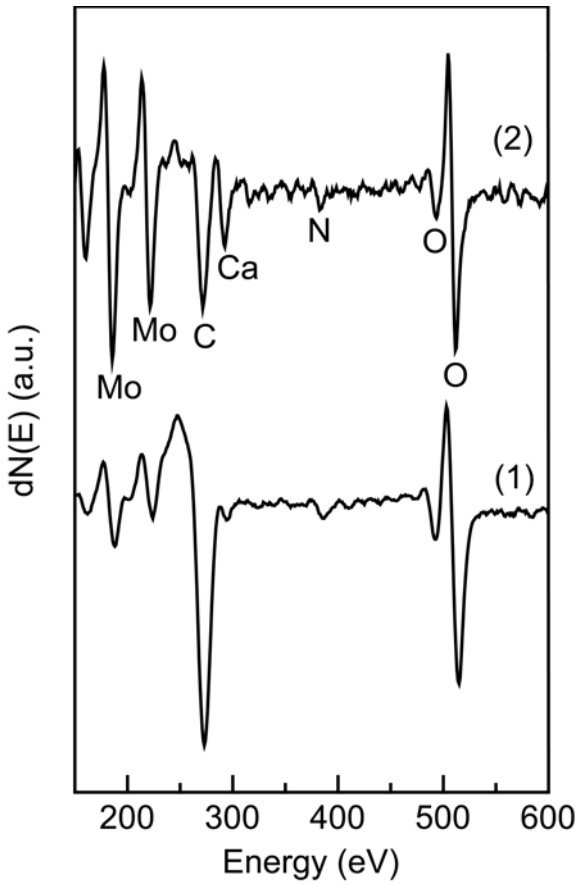


Figure 4. Auger analyses of the Mo substrate in a region close to the drop edge after the spreading of GTi glass for two hours under (1) nonreactive ($p(O_2)=10^{-16}$ atm) and (2) reactive ($p(O_2)=10^{-20}$ atm) conditions. A much larger Ca peak can be observed after spreading under reactive conditions.

**Reactive spreading ($p(O_2)<10^{-19}$ atm).** The spreading velocities are similar to those of the nonreactive case. For most experiments, with decreasing contact angle, the liquid front exhibited a discontinuous ("stick-slip") movement: it stopped, jumped, and resumed spreading (Figure 5).

The final contact angles were larger than those for the nonreactive case and decreased with the addition of $TiO_2$ (Figure 3).

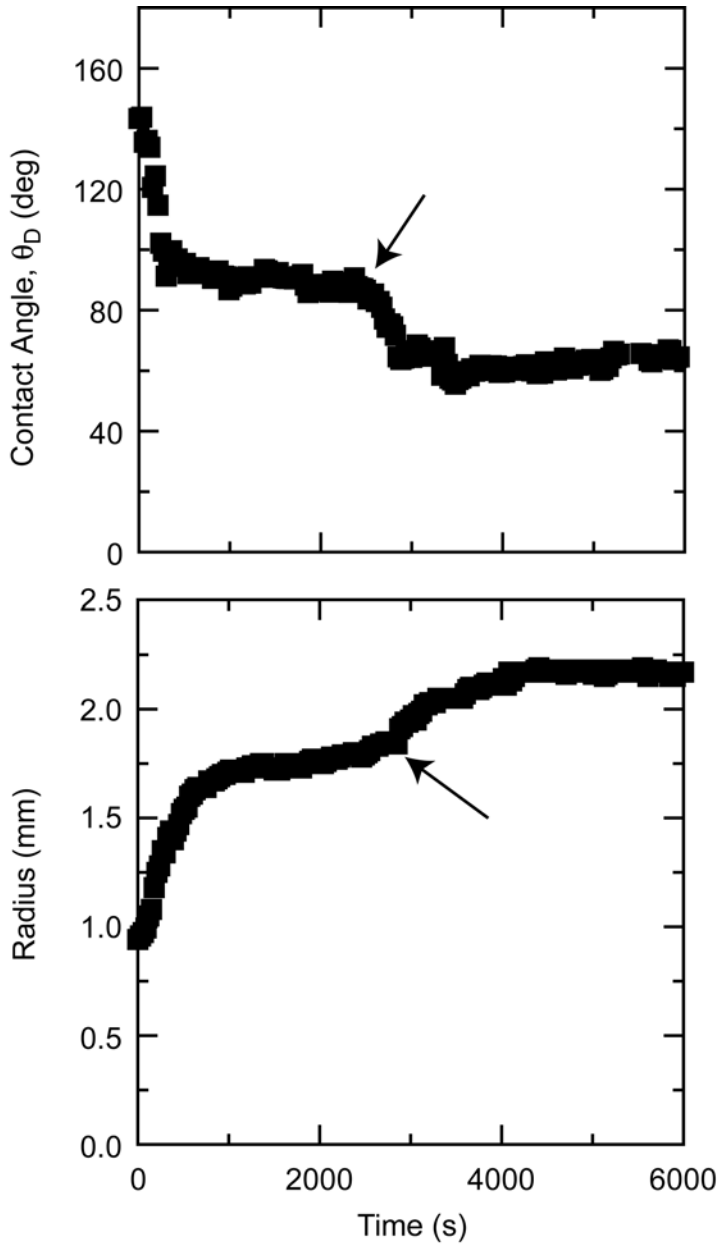


Figure 5. Typical time evolution of the contact angle and drop radius for a glass spreading on Mo at 1200°C under reactive conditions. The curve corresponds to a G glass spreading under an oxygen partial pressure of $10^{-20}$ atm. After ~1,000 s, the drop spreading stopped and resumed movement shortly afterwards (arrows).

After cooling, discontinuous islands of reaction product can be observed at the glass/metal interface. The islands were tens of microns wide and less than 1 μm thick and concentrate in a narrow band (~50 μm wide) around the solid-liquid-vapor triple junction (Figure 6). The rest of the glass metal interface is free of reaction product. EDS analysis showed that these islands are composed of a Mo-Si intermetallic. The formation of $Mo_3Si$ at the interface between silica-containing ceramics and molybdenum under reducing conditions has been previously described.[28] Submicron glass drops ahead of the glass front can also be observed (Figure 6). These glass drops form due to evaporation-condensation of the glass.[29] As in the nonreactive case, no Mo was detected in the glass drops.

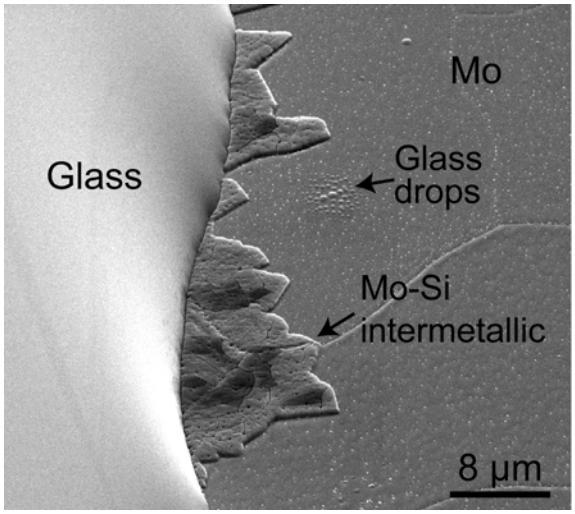


Figure 6. SEM micrograph of the drop edge after spreading of a GTi glass on Mo for 4 hours. The oxygen partial pressure during the experiment was $10^{-23}$ atm (reactive conditions). Islands of reaction product are clearly visible at the triple junction.

In contrast to the nonreactive case, triple-line ridges (~20 nm in height) were observed after removing the glass drop (Figure 7), and grain boundary grooves were clearly visible at the glass/metal interface and on the free Mo surface (Figure 8). The groove widths at the glass/Mo

interface or at the free Mo surface close to the triple line are very similar, ~0.8–1 μm after 2 hours at 1200°C (Table 2). However, the width of the groove clearly decreased as we moved away from the triple junction towards the edge of the Mo substrate. Similar groove sizes were observed for glasses with or without $TiO_2$.

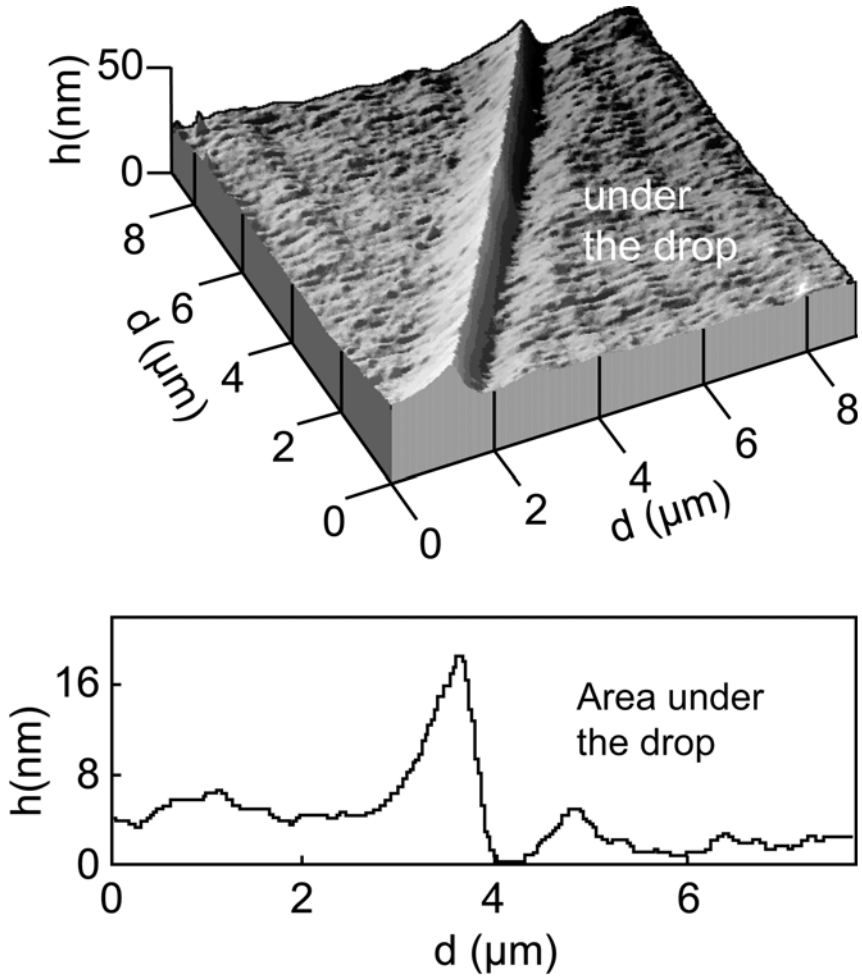


Figure 7. AFM image and corresponding profile of the triple-line ridge formed after spreading a G glass (without $TiO_2$) on Mo for 2 hours in an atmosphere with an oxygen partial pressure of $10^{-22}$ atm. The glass drop was removed to scan the area around the triple junction. The shape of the ridge corresponds to an evolution controlled by interfacial diffusion.

After removing the glass drops, a Ca peak much stronger than that for the non-reactive case was observed by Auger spectroscopy at the glass/metal interface and on the free Mo surface (Figure 4). Peak height decreased as we moved away from the drop.

| $p(O_2)$ (atm) | Glass | Time (min) | *w* solid-liquid (μm) | *w* solid-vapor (μm) |
|---|---|---|---|---|
| $3\times10^{-20}$ | G | 120 | 0.8±0.1 | 0.6±0.2 |
| $3\times10^{-20}$ | GTi | 120 | 0.7±0.1 | 0.7±0.1 |
| $1\times10^{-22}$ | G | 120 | 1.0±0.1 | 0.8±0.2 |
| $6\times10^{-22}$ | GTi | 120 | 1.0±0.1 | 0.7±0.1 |

**Table 2.** Measured groove widths, *w*, at the solid/liquid and solid/vapor interfaces.[†]

## Discussion

**Glasses.** The measured surface energies are of the order of those reported for silicate glasses of similar compositions.[24] Both the atmosphere and the small $TiO_2$ additions have a minor effect on the surface tension of the glass. It was already reported that titanium ions have a limited effect on the surface energy, as they have a strong tendency to surround themselves with oxygen ions

[†]The measurements in the solid/vapor interface were taken in an area ~500 μm around the edge of the drop. The groove widths decrease noticeably when the measurements are moved further away from the drop towards the edge of the substrate.

whether in the interior or on the surface of the glass.[30] However, most of the experimental studies have been done under conditions that are far less reducing than those used in this work. It is not clear if the decrease in surface energy with decreasing $p(O_2)$ is due to changes in glass structure or to $H_2$ adsorption from the atmosphere. For the purpose of spreading analysis, the important point is that the small $TiO_2$ additions do not have a strong effect on the surface tension and viscosity of the molten glass[25, 31], allowing a straightforward comparison of the glass-spreading data with and without titania at different oxygen activities.

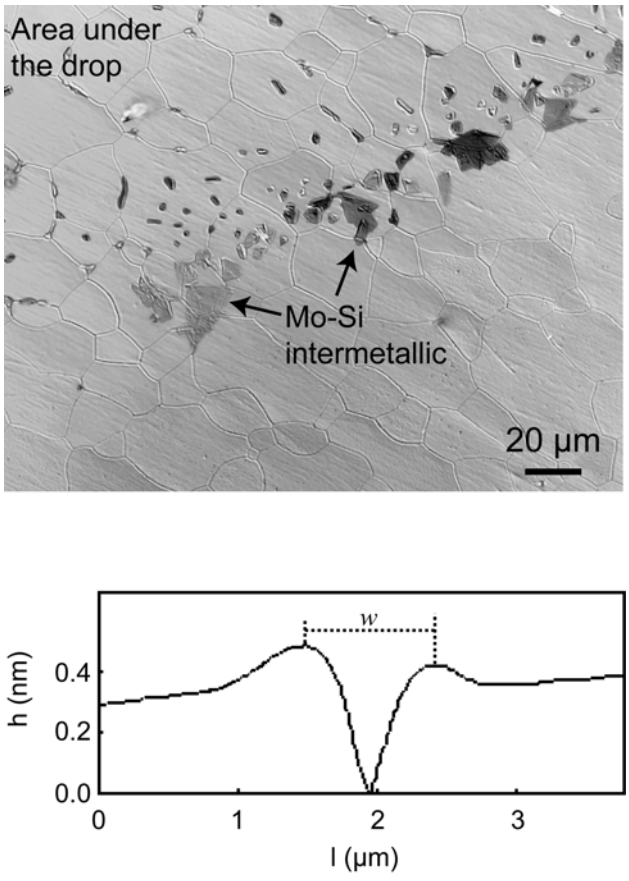


Figure 8. Optical micrographs and AFM profile of a grain boundary groove forming at the glass/metal interface under reactive conditions. The optical micrograph was taken after removing a G glass drop that was heated at 1200°C for 2 hours in a $p(O_2)$ of $10^{-22}$ atm. Molybdenum silicide islands are visible in the area close to the triple junction. The groove widths are similar under the drop and on the free Mo surface. The shape of the grooves (the presence of humps at both sides) corresponds to grooving controlled by diffusion.

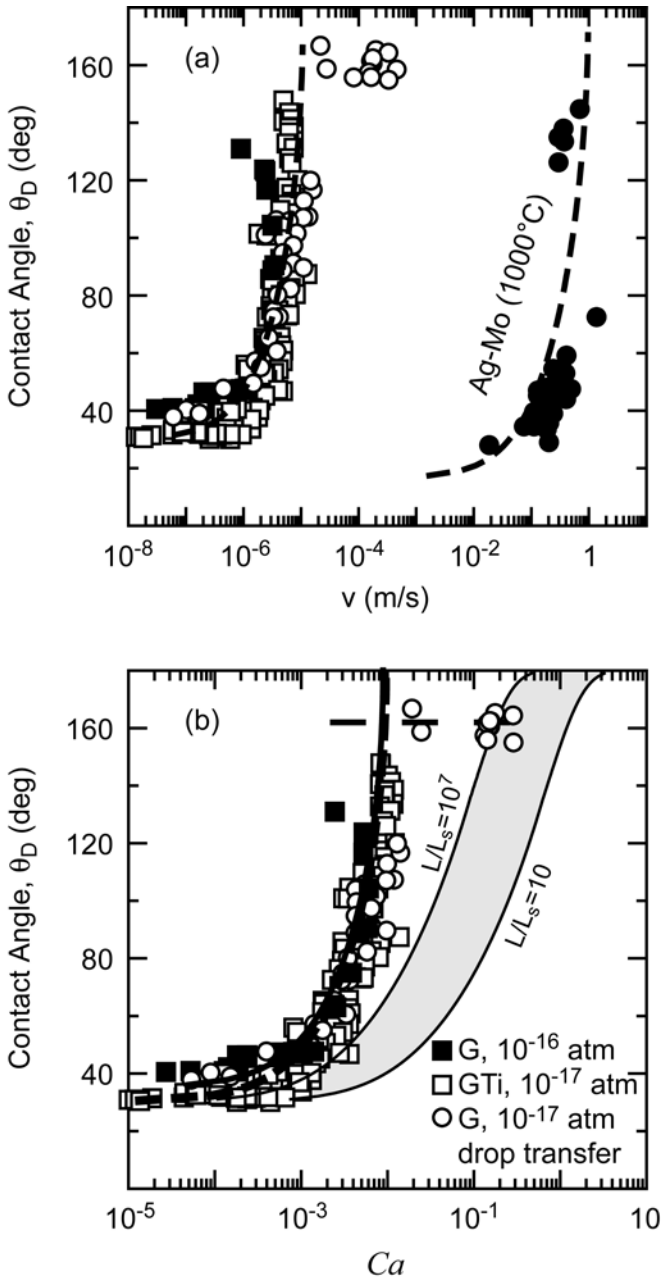


Figure 9. (a) Plot of the velocity of spreading vs. dynamic contact angle for glasses on Mo under nonreactive conditions. For comparison, data corresponding to the spreading of liquid silver on Mo at 1000°C are also presented.[34] This is a system with partial wetting where no chemical reaction or measurable interdiffusion occurs during spreading.[34] Glass spreading is orders of magnitude slower. (b) Glass data are used to create a plot of the capillary number vs. dynamic contact angle. The shadowed area delimits the expected kinetics for spreading controlled by the viscous impedance (Eq. 2–3). Fittings of the data to the molecular-kinetic model (discontinuous line, Eq. 5) and the Cherry and Holmes equation (continuous line, Eq. 6) are also presented. The fittings use similar adsorption distances for the metal/metal and the glass/metal systems, $\lambda \approx 2$–$4$ Å, but the wetting activation energies are of the order of 230–300 kJ/mol for glasses, and 100–120 kJ/mol for liquid silver.[34]

**Nonreactive spreading.** Since our measurements suggest that the addition of 3 mol% $TiO_2$ has a negligible effect or, at the higher oxygen activities, even increases slightly the surface energy of the molten glass, the observed decrease of the equilibrium contact angle for glasses with $TiO_2$ additions can only be explained by the preferential adsorption of $TiO_x$–species at the solid/liquid interface. This does not preclude adsorption of $TiO_x$ at the solid/vapor interface. but in order to decrease the contact angle, adsorption has to result in a larger decrease of the solid-liquid interfacial energy. Copley and Rivers[32] had already shown that $TiO_2$ additions decrease the contact angle of silicate glasses on Pt (albeit these experiments were performed in air), and there is ample evidence of adsorption of Ti-species at the interface between liquid metals and solid oxides that has been attributed to their polar nature.[17, 33]

As can be expected from their much larger viscosity, the spreading times for the molten oxide drops are orders of magnitude larger than for liquid metals at similar temperatures (Figure 9).[2, 34, 35] This fact is consistent with a spreading kinetics controlled by the viscous dissipation in the drop, a situation that is usually described using continuous hydrodynamic models. Hydrodynamic theories search for a universal relationship between the dynamic contact angle and the capillary number, $Ca = v\eta/\gamma_{lv}$ ($v$ is the velocity of the triple junction and $\eta$ the liquid viscosity), that is typically written in the form[8-10]:

$$g(\theta_D) - g(\theta_0) = Ca \ln\left(\frac{L}{L_s}\right) + \mathrm{O}(Ca) \qquad (2)$$

where $g(\theta)$ is a function of the contact angle, $L$ is a characteristic capillary length, and $L_s$ is the slip length; $L_s$ corresponds to a thickness of the meniscus immediately adjacent to the solid wall over which the "no-slip" boundary condition of classical hydrodynamics is relaxed; $\theta_0$ is the equilibrium contact angle. At a first approximation, the expected behavior from the different hydrodynamic models is very similar. For dynamic contact angles smaller than 135°, the behavior can be described using the well-known equation.[5, 8-10]

$$Ca = \frac{1}{9\ln\left(\frac{L}{L_s}\right)}\left(\theta_D^3 - \theta_0^3\right) \qquad (\theta_D \leq 135°) \qquad (3)$$

It is usually accepted that the spreading of organic liquids with viscosities ranging from $10^{-3}$ to $10^{1}$ N·s/m$^2$ can be described using hydrodynamic models, except perhaps in instances of very fast forced wetting.[10, 36] However, in the plot of capillary number vs. dynamic contact angle, glass data are much slower than expected from Eqs (2) and (3) using values for L/Ls with physical meaning (see the shadowed area in Figure 9). The same has been observed for the spreading of liquid metal drops.[37] *This suggests that high-temperature spreading is controlled by local energy dissipation at the triple junction (the friction of the triple line).* Nevertheless, viscosity should still be playing a role, as the solid/liquid interactions (the works of adhesion) are expected to be similar for the glass/metal and metal/metal systems,[34] but glass spreading is orders of magnitude slower. Blake has proposed a molecular-kinetic model that takes into account both chemical and viscous contributions to the local dissipation, and where the driving force for wetting is the out-of-balance interfacial tension force: $\gamma_{lv}(\cos\theta_0 - \cos\theta_D)$.[4] The model is an extension of reaction-rate theories[38] in which molecules of an advancing fluid displace

molecules of a receding one on adsorption sites on the substrate. The two critical parameters in the model are λ, the distance between adsorption sites; and $\Delta G_w$, a wetting activation energy. It can be assumed that in the case of a liquid advancing against a gas of negligible viscosity, $\Delta G_w$ has two components:

$$\Delta G_w = \Delta G_s + \Delta G_{vis} \quad (4)$$

where $\Delta G_s$ is the contribution arising from the retarding influence of the solid alone (a chemical contribution related to the interactions between the solid and the liquid), and $\Delta G_{vis}$ a viscous contribution that arises from the interactions with other liquid molecules and that is identified with the activation of free energy for bulk flow. According to the model, the relationship between the velocity of the liquid front and the dynamic contact angle can be written as[4]:

$$Ca = \frac{2\eta\lambda kT}{h\gamma_{lv}} e^{-\frac{\Delta G_\omega}{NkT}} \left( \sinh\left( \frac{\lambda^2 \gamma_{lv}}{2kT} \left( \cos(\theta_0) - \cos(\theta_D) \right) \right) \right) \quad (5)$$

Where N is Avogadro's number and *k* and *h* are the Boltzmann and Planck constants respectively. The data can be fitted to Eq (5) using adsorption distances of the order of interatomic distances (1–4 Å) and wetting activation energies of ~230–300 kJ/mol (Figure 9) that are of the order of the activation energy for viscous flow in the glasses (~ 290 kJ/mol). These results reflect a situation in which the viscous interactions between the liquid molecules are stronger than the solid/liquid forces, and the viscous contribution dominates the wetting

activation energy. The process will be equivalent to Cherry and Holmes' description[39] of spreading of polymers with very large viscosities ($10^2$ N·s/m$^2$, similar to our glasses). Their model is very similar to that of Blake.[4] They made a parallel between spreading and the reaction rate theory of viscosity[38] and assumed that the spreading velocity was determined by the movement of "flow units" over arbitrary energy barriers on the solid surface. From their equations, the following relationship between the dynamic contact angle and the capillary number can be deduced.[4]

$$Ca = \frac{\lambda^2 \delta \gamma_{lv}}{\mathrm{v}} \left( \cos\theta_0 - \cos\theta_D \right) \qquad (6)$$

where δ is the length of the unit flow (typically the molecule) in the direction parallel to the wetting line, and v is the volume of the unit flow (~$3 \cdot 10^{-26}$ m$^3$, according to the data in Figure 1). Equations (5) and (6) are equivalent when $\theta_D \rightarrow \theta_0$ and $\lambda \approx \delta$. Fitting the data to equation (6) and taking $\delta = \mathrm{v}^{1/3}$ results in λ ≈3-4 Å, which again is of the order of interatomic distances, as can be expected for the distances between adsorption sites on the solid surface.

It is interesting to compare the calculated wetting activation energies and corresponding equilibrium frequencies $\kappa_w^0 = \frac{kT}{h} e^{\frac{-\Delta G_w}{NkT}}$ for different systems. For organic liquids at room temperature, the reported activation energies vary between 10–50 kJ/mol ($\kappa_w^0 = 10^4 - 10^{11}\ \mathrm{s}^{-1}$)[4]; for liquid metals, ~$10^2$ kJ/mol ($\kappa_w^0 = 10^9 - 10^{10}\ \mathrm{s}^{-1}$)[37]; and for our glasses, $\Delta G_w$ = 230–300 kJ/mol ($\kappa_w^0 = 10^3 - 10^5\ \mathrm{s}^{-1}$). For liquid metals, the activation energies for viscous flow are very small (1–

10 kJ/mol) and $\Delta G_{vis} << \Delta G_s$. The main contribution to the wetting activation energy is the solid/liquid interaction, and the spreading mechanism is parallel to surface diffusion.[34, 35, 37, 38] On the other hand, for molten oxides, as for highly viscous polymers, the contribution to the local dissipation from the solid/liquid interactions is relatively small, and the triple-line friction is determined by viscous interactions between liquid molecules: $\Delta G_w \approx \Delta G_{vis}$.

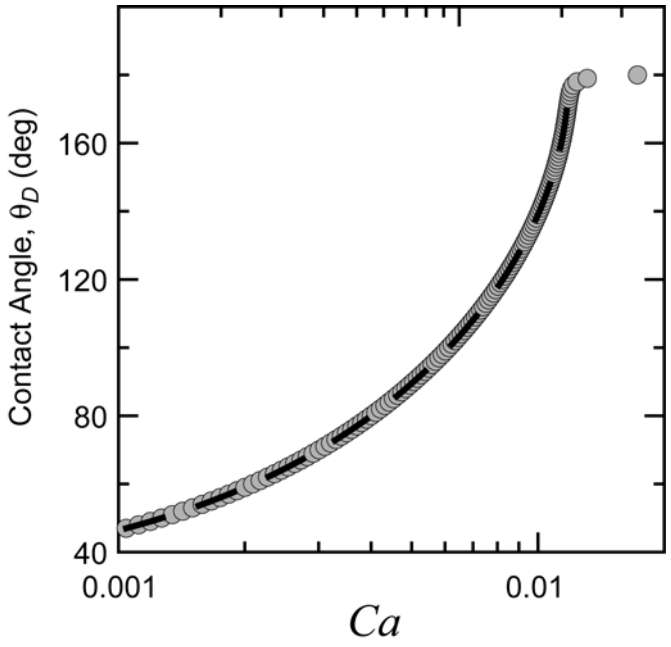


Figure 10. Expected variation of the dynamic contact angle ($\theta_D$) with capillary number (*Ca*) according to the molecular dynamic model using different definitions of the spreading driving force: Eq. 5 (dashed line) or Eq. 11 (circles). It can be observed that for the same parameters ($\lambda$ = 2 Å, $\eta$ = 350 N·s/m$^2$, $\theta_0$ = 30°) both curves are almost identical, but Eq. 11 reproduces qualitatively the "plateau" observed in the experiments at very high dynamic contact angles.

Our drop transfer data deviate from the behavior predicted by equation (5) when the dynamic contact angle approaches 180° (Figure 9). Similar deviations have been observed in other systems[4] and have been attributed to the existence of additional driving forces besides the unbalanced surface tension or to the increasing contribution of molecules from the liquid/vapor

interface to the flux of advancing liquid.[4] The difference between the experimental and predicted behavior can also be due to the way in which the driving force for the spontaneous spreading of the small drops is defined. In the original formulation of Blake's model, the driving force for spreading is written as the out-of-balance interfacial tension force $\gamma_{lv}(\cos\theta_0 - \cos\theta_D)$.[4] Another possibility is to write the driving force as the decrease in free energy of the system as the drop advances towards the equilibrium contact angle. Using the most simplistic approach, the variation of free energy is due to a variation in the area of the different interfaces that can be written as:

$$dG = \gamma_{sv} dA_{sv} + \gamma_{sl} dA_{sl} + \gamma_{lv} dA_{lv} \tag{7}$$

where $dA_i$ is the variation in area of the respective interfaces as the drop spreads. If all the surfaces have constant curvature:

$$dA_{sv} = -dA_{lv} = 2\pi r dr \tag{8}$$

$$dA_{lv} = \frac{4\pi r(1-\cos\theta)}{\sin^2\theta} dr - 2\pi r^2 \frac{(1-\cos\theta)^2}{\sin^3\theta} d\theta \tag{9}$$

where $r$ is the radius of the drop base and $\theta$ the contact angle. Because the volume of the drop is constant, and assuming that the shape of the drop is always a spherical cap, it is possible to write $r$ as a function of the contact angle. Then the decrease of free energy by unit length of the wetting line during the displacement of the triple junction at distance $dr$ can be written as:

$$w = \frac{1}{2\pi r}\frac{dG}{dr}dr \qquad (10)$$

Following Blake's approach, the relationship between the spreading velocity and the dynamic contact angle can be written as[4]:

$$Ca = \frac{2\eta\lambda kT}{h\gamma_{lv}} e^{-\frac{\Delta G_\omega}{NkT}} \left( \sinh(\frac{\lambda^2 w}{2kT}) \right) \qquad (11)$$

In Figure 10, the resulting wetting kinetics are plotted and compared with those calculated using equation (5). The fitting parameters calculated from equations (5) and (1) are almost identical, but equation (11) reproduces the behavior at large contact angles better. This is due to the fact that as $r \rightarrow 0$ ($\theta \rightarrow \pi$), $w$ increases faster than $\gamma_{lv}(\cos\theta_0 - \cos\theta_D)$.

**Reactive spreading.** As expected from Equation (1), a chemical reaction took place between the glass and the metal at oxygen partial pressures below $10^{-19}$–$10^{-20}$ atm. Most of the reaction product could be seen in the form of small islands around the triple line, which indicates that the glass front was spreading mostly on an unreacted metal surface, and the reaction product formed after the liquid front stopped (Figure 5). Consequently, the maximum spreading speeds in the reactive and nonreactive cases are very similar, and the spreading mechanisms are the same (Figure 11). When the speed of the liquid front approaches zero, then there is time for the reaction product to nucleate at the triple junction where equilibration with the surrounding atmosphere occurs faster than at the center of the drop.

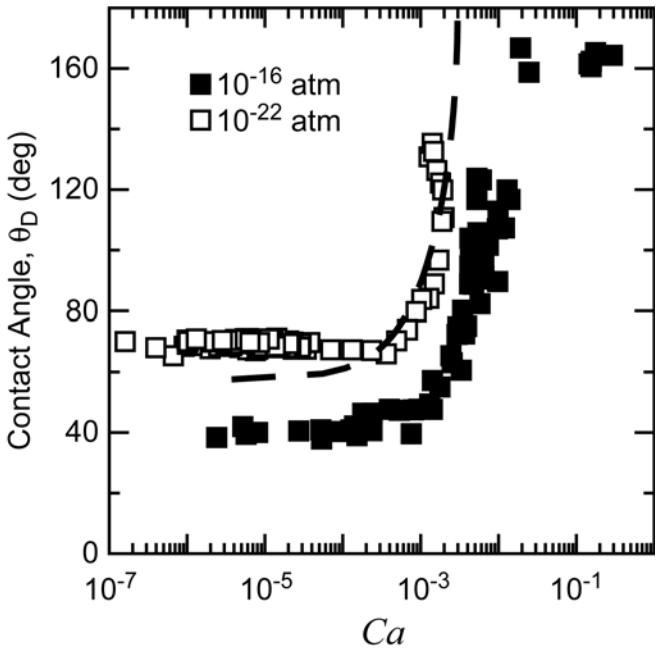


Figure 11. Comparison of the capillary number vs dynamic contact angle behavior for the G glass (without $TiO_2$) spreading under reactive ($p(O_2) = 10^{-22}$ atm) and nonreactive ($p(O_2) = 10^{-16}$ atm) conditions. The spreading kinetics are very similar. Fitting of the reactive data to a molecular-kinetic model (Eq. 5) is also presented ($\lambda \approx$ Å, $\Delta G_w \approx 250$ kJ/mol, $\theta_0 \approx 57°$). The fitting suggests that the mechanisms controlling spreading in the reactive and nonreactive cases are very similar and that spreading in the reactive case stopped at angles slightly higher due to the formation of ridges and subsequent pinning of the liquid front.

Our experiments clearly show that at very low oxygen activities, the presence of glass enhances mass transport at the metal surface and at the metal/glass interface, and grain boundary grooves grow large enough to become visible. The grooves are wider at the metal/ceramic interface and on the metal surface close to the liquid front. Such behavior suggests that enhanced transport is due to adsorption of glass species at very low oxygen activities (or in atmospheres with higher $H_2$ content). Auger analyses have shown a strong Ca peak at the glass/metal interface and on the free Mo surface (Figure 6). Similar groove widths have been measured for glasses

with and without Ti. The corresponding interfacial diffusivities can be estimated using measured groove widths. According to Mullins, the groove width ($w$) should evolve with time as[40]:

$$w = 4.6\left(\frac{B_i t}{2}\right)^{1/4} \tag{12}$$

where $B_i$ is the corresponding interfacial transport coefficient:

$$B_i = \frac{\omega D_i \gamma_i \Omega}{kT} \tag{13}$$

with $\omega D_{si}$ being the width-diffusivity product for the specific interface; $\Omega$, the atomic volume; and $k$, Boltzmann's constant. For the observed groove widths (~ 1 μm wide after 2 hours), the calculated $B_{sv} \approx B_{sl} \approx 6.2 \cdot 10^{-31}$ $m^4/t$. These values are slightly larger than expected from reported transport coefficients for pure Mo[41], as they correspond to a surface with some degree of adsorption on it.

Faster atomic transport results in the formation of triple-lines ridges by atomic migration near the contact line.[19] The driving force for triple-line ridge formation is the equilibration of interfacial forces perpendicular to the substrate. For most low-temperature systems, the vertical component of the surface-tension-induced force at the triple junction is resisted by elastic distortions of the solid. It is then accurate to describe the substrate as ideally rigid and insoluble and the liquid as moving on a flat surface; however, at high temperatures, local diffusion or solution/precipitation can occur, providing the mechanism for ridge formation. Once the ridge

forms, the triple junction will remain attached to it. If ridge movement is slow compared with experimental times, the triple line will practically stop moving unless a sudden perturbation or liquid evaporation drives the macroscopic contact angle outside a stability range that depends on the ridge orientation, causing the wetting front to break away[19]; this explains the observed stick-slip motion when the contact angles approach the stationary value. A time scale exists in which a ridge is attached at the triple line, and the spreading kinetics is dictated by the rate at which the ridge moves (regime II or III spreading).[19]

Due to the negligible solubility of metallic Mo on the glass, ridges should evolve by interfacial diffusion. This is confirmed by the ridge shape (the existence of a bump close to the advancing ridge in the solid/liquid interface).[19] Under these conditions, the maximum speed for a ridge can be written as[19]:

$$v_{ss}^{adv} = B_{sv}\left(\frac{y'_{sv}(0)}{h}\right)^3 \qquad (15)$$

where $y'_{si}(0)$ is the slope of the ridge at the junction for the appropriate interface, and $h$ is the ridge height. The maximum velocity for a 20 nm ridge with a finite slope < 0.5 (typical for the observed ridges) will be ~$10^{-8}$ m/s. These velocities are one to three orders of magnitude slower than those observed, supporting the idea that once a ridge forms and grows to a measurable height, spreading stops unless the triple junction breaks away from the ridge and resumes its movement. There are three additional reasons that support the idea that spreading velocities are not controlled by ridge movement, even in the reactive case:

i) The maximum speeds are similar for reactive and nonreactive spreading, and no ridge was observed after nonreactive spreading.

ii) The extent of ridge growth ($\Delta h$ ) escalates with the drop size and change in angle ($\Delta h \propto r[F(\theta_f) - F(\theta_i)] \propto \Delta r$, where $r$ is the radius of the drop base, and $\Delta r$ is the distance traveled by the liquid front).[19] It is highly unlikely that a ridge that has grown to be ~20 nm in height would have traveled a distance of the order of several millimeters with the liquid front; it is most likely to have only traveled for a distance of a few tens of nanometers.

iii) When ridge growth is controlled by interfacial diffusion, ridge formation is stable only inside a range of dynamic contact angles around the equilibrium value. This range is defined by the physical characteristics of the system. Using the result for a symmetric system as a guide, the range for stable ridge growth is[19, 42]:

$$\theta_{1D} \pm \Delta\theta = \theta_{1D} \pm \frac{\gamma_{lv}}{6\gamma_{sv}} \qquad (16)$$

If $\gamma_{sv} \approx \gamma_{sl} \approx 2$ J/m$^2$ and $\gamma_{lv} \approx 0.49$ J/m$^2$ [43], then $\Delta\theta \approx 2°$. Small corrections are expected when using the exact asymmetric surface energies. Ridges can nucleate outside the stability range (imperfections on the substrate surface such as roughness, scratches, or grain boundaries can act as nucleation centers). However, in that case, the ridge will have to decrease in size in order to move with the liquid front[19], or the drop will stop and then break away from the ridge and resume motion. If glass species adsorb at the solid/vapor and solid/liquid interfaces, decreasing the corresponding energies, the ridge stability range will increase.

The picture that emerges for the reactive case is that of a liquid front moving on a flat unreacted surface. When spreading slows down, a ridge can form either because it is nucleated by defects of the substrate surface, or because the critical stability range for ridge formation has been reached. When the ridge reaches a critical height of ~10–20 nm, its speed will be so low that experimental spreading of the liquid front stops, unless it can break away from the ridge and resume motion. Once the spreading velocity approaches zero, the reaction product will nucleate at the triple junction.

The conventional view of high-temperature reactive spreading is that both the reaction products and the liquid front advance together.[1, 21] The results discussed in this paper agree with other results recently published for the spreading or reactive brazes on ceramics, which indicate that this is not always the case.[33] A comprehensive theory of reactive spreading should start by dividing the process into its constitutive steps (fluid flow, adsorption, ridging, and compound formation), and determining the relative kinetics of each step to verify which step drives wetting, and which controls spreading kinetics.[17] The key question is the balance between the spreading and the reaction or interdiffusion kinetics. The analysis is parallel to studies on the effect of adsorption on spreading kinetics. Depending on the balance between adsorption kinetics and spreading kinetics, spreading can occur before all the interfaces can reach their equilibrium amount of adsorbate; for example, in the dry spreading case, the absence of the equilibrium amount of adsorbate in the surface of the substrate ahead of the liquid front results in enhanced wetting.[5] In the glass/metal systems most of the spreading occurs previous to reaction and its kinetics is controlled by the same mechanisms the operate that for the non-reactive case.

Against the commonly accepted ideas that suggest that chemical reaction enhances wetting, we have not observed a substantial decrease in the contact angles at low oxygen partial pressures. In equations (3) and (5), the driving forces for spreading are written in terms of the differences between the dynamic and the equilibrium contact angles, given by the well-known Young's equation. In the nonreactive case, all the interfacial energies and driving forces involved are well defined, whereas in the reactive case, it is required to define an interfacial energy for the metastable unreacted interface between the glass and the metal. Both the spreading speeds and the final contact angles are very similar in the reactive and nonreactive cases, suggesting that equilibrium interfacial energies of the nonreactive systems and those of the metastable interfaces under reactive conditions are similar. That means that the work of separation between the unreacted phases is similar to the thermodynamic work of adhesion between the phases in equilibrium under nonreactive conditions. However, the final contact angle in the reactive system should be that of the glass on the reaction product $Mo_3Si$, but due to the roughness of the reaction phase, it is not possible to know if this final angle is the intrinsic value for the glass on the silicide.

## Conclusions

The spontaneous spreading of silicate glass drops on Mo substrates is much slower than predicted by hydrodynamic models, suggesting that the spreading velocity is controlled by the triple-junction friction, not by viscous dissipation in the bulk liquid. Furthermore, viscous interactions between liquid molecules are the main contribution to triple-line frictions. This is similar to the mechanism that controls spreading of highly viscous polymers.

A comparison between nonreactive and reactive cases suggests that the driving forces and controlling mechanisms are similar. The main difference is that enhanced interfacial diffusion under reactive conditions results in the formation of triple-line ridges that eventually stop spreading and promote a characteristic stick-slip motion. These results underline the need for a comprehensive new model that describes high-temperature reactive spreading and that should divide the process into its constitutive steps; by determining the relative kinetics of each step, the new model can then define the mechanisms that drive and control reactive spreading in each system.

**Acknowledgement.** This work was supported by the Director, Office of Science, Office of Basic Energy Sciences, Division of Materials Sciences and Engineering, of the U.S. Department of Energy under Contract No. DE-AC03-76SF00098. S. Lopez-Esteban was partly supported by a Fulbright Grant and wishes to thank the Spanish Ministry of Education, Culture and Sports for financial sponsorship.

## References

(1) Eustathopoulos, N.; Nicholas, M. G.; Drevet, B., *Wettability at high temperatures*. Pergamon: Amsterdam ; New York, 1999.

(2) Berg, J. C., *Wettability*. M. Dekker: New York, 1993.

(3) Gennes, P.-G. d.; Quere, D.; Brochard-Wyard, F., *Capillarity and wetting phenomena; drops, bubbles, pearls, waves*. Springer-Verlag: New York, 2004.

(4) Blake, T. D. In Wettability: Berg, J. C. Ed; Marcel Dekker Inc.: New York, 1993; p 251.

(5) de Gennes, P. G. *Rev. Mod. Phys.* **1985,** 53, 827.

(6) De Coninck, J.; de Ruijter, M. J.; Voue, M. *Current Opinion in Colloid & Interface Science.* **2001,** 6, 49.

(7) de Ruijter, M. J.; Blake, T. D.; De Coninck, J. *Langmuir* **1999,** 15, 7836.

(8) Cox, R. G. *J. Fl. Mech.* **1986,** 168, 169.

(9) Voinov, O. V. *Izvestiya Akademii Nauk SSSR, Mekhanika Zhidkosti i Gaza.* **1976**, 76.

(10) Kistler, S. F., In Wettability: Berg, J. C. Ed; Marcel Dekker Inc.: New York, 1993; p 311.

(11) de Ruijter, M. J.; De Coninck, J.; Oshanin, G. *Langmuir.* **1999,** 15, 2209.

(12) de Ruijter, M. J.; De Coninck, J.; Blake, T. D.; Clarke, A.; Rankin, A. *Langmuir* **1997,** 13, 7293.

(13) Blake, T. D.; De Coninck, J. *Adv. Coll. Interf. Sci.* **2002,** 96, 21.

(14) Weirauch, D. A.; Lazaroff, J. E.; Ownby, P. D. *J. Amer. Ceram. Soc.* **1995,** 78, 2923.

(15) Lazaroff, J. E.; Ownby, P. D.; Weirauch, D. A. *J. Amer. Ceram. Soc.* **1995,** 78, 539.

(16) Adams, R. B.; Pask, J. A. *J. Amer. Ceram. Soc.* **1961,** 44, 430.

(17) Saiz, E.; Cannon, R. M.; Tomsia, A. P. *Acta Mater.* **2000,** 48, 4449.

(18) Copley, G. J.; Rivers, A. D. *J. Mat. Sci.* **1975,** 10, 1291.

(19) Saiz, E.; Tomsia, A. P.; Cannon, R. M. *Acta Mater.* **1998,** 46, 2349.

(20) Saiz, E.; Tomsia, A. P.; Cannon, R. M. *Scripta Mater.* **2001,** 44, 159.

(21) Eustathopoulos, N., *Acta Mater.* **1998,** 46, 2319.

(22) Hansen, F. K. *Drop Image*, Rame-Hart Inc: Mountain Lakes, USA, 2002.

(23) Weyl, W. A., *Coloured Glasses*. Society of Glass Technology, Sheffield, England: 1976.

(24) Weirauch, D. A.; Ziegler, D. P. *J. Amer. Ceram. Soc.* **1996,** 79, 920.

(25) Kawai, Y.; Shiraishi, Y., *Handbook of Physico-chemical Properties at High Temperatures*. The Iron and Steel Institute of Japan (ISIJ): 1988.

(26) *Outokumpu HSC Chemistry for Windows*, 1.10; Outokumpu Research Oy: Pori, Finland, 1993.

(27) Radigan, W.; Ghiradella, H.; Frisch, H. L.; Schonhorn, H.; Kwei, T. K. *J. Coll. Interf. Sci.* **1974,** 49, 241.

(28) Heikinheimo, E.; Kondentsov, A.; van Beek, J. A.; Klomp, J. T.; van Loo, F. J. J. *Acta Metal. Mat.* **1992,** 40, S111.

(29) Copley, G. J.; Rivers, A. D.; Smith, R. *J. Mat. Sci.* **1973,** 8, 1049.

(30) Stanworth, J. E., *Physical properties of glass*. Clarendon Press: Oxford,, 1950.

(31) Hocking, L. M.; Rivers, A. D. *J. Fluid Mech.* **1982,** 121, 425.

(32) Copley, G. J.; Rivers, A. D. *J. Mat. Sci.,* **1975,** 10, 1291.

(33) Gremillard, L.; Saiz, E.; Chevalier, J.; Tomsia, A. P. *Z. fur Metall.* **2004,** 95, 261.

(34) Rauch, N.; Saiz, E.; Tomsia, A. P. *Z. fur Metall.* **2003,** 94, 233.

(35) Saiz, E.; Hwang, C. W.; Suganuma, K.; Tomsia, A. P. *Acta Mater.* **2003,** 51, 3185.

(36) Brochard-Wyart, F.; de Gennes, P. G. *Adv. Coll. Interf. Sci.* **1992,** 39, 1.

(37) Saiz, E.; Tomsia, A. P., *Nature Materials*, **2004**, 3, 903.

(38) Glasstone, S.; Laidler, K. J.; Eyring, H., *The theory of rate processes; the kinetics of chemical reactions, viscosity, diffusion and electrochemical phenomena*. McGraw-Hill Book Company Inc.: New York, 1941; p 611.

(39) Cherry, B. W.; Holmes, C. M., *Journal of Colloid and Interface Science* **1983,** 94, 470.

(40) Mullins, W. W. *J. Appl. Phys.* **1957,** 28, 333.

(41) Seebauer, E. G.; Allen, C. E. *Prog. Surf. Sci.* **1995,** 49, 265.

(42) Mullins, W. W. *Acta Mater.* **1958,** 6, 414.

(43) Keene, B. J. *Inter. Mat. Rev.* **1993,** 38, 157-192.

## Table of Contents Graphic